Selected Wheat Seed Defense Proteins Exhibit Competitive Binding to Model Microbial Lipid Interfaces

Michael R. Sanders,[†,‡] Luke A. Clifton,[§] Cameron Neylon,[§] Richard A. Frazier,[‡] and Rebecca J. Green*[†]

[†]Reading School of Pharmacy and [‡]Department of Food and Nutritional Sciences, University of Reading, P.O. Box 226, Whiteknights, Reading RG6 6AP, United Kingdom

[§]ISIS Spallation Neutron Source, Science and Technology Facilities Council, Rutherford Appleton Laboratory, Harwell Science and Innovation Campus, Didcot, Oxfordshire OX11 OQX, United Kingdom

ABSTRACT: Puroindolines (Pins) and purothionins (Pths) are basic, amphiphilic, cysteine-rich wheat proteins that play a role in plant defense against microbial pathogens. This study examined the co-adsorption and sequential addition of Pins (Pin-a, Pin-b, and a mutant form of Pin-b with Trp-44 to Arg-44 substitution) and β-purothionin (β-Pth) model anionic lipid layers using a combination of surface pressure measurements, external reflection FTIR spectroscopy, and neutron reflectometry. Results highlighted differences in the protein binding mechanisms and in the competitive binding and penetration of lipid layers between respective Pins and β-Pth. Pin-a formed a blanket-like layer of protein below the lipid surface that resulted in the reduction or inhibition of β-Pth penetration of the lipid layer. Wild-type Pin-b participated in co-operative binding with β-Pth, whereas the mutant Pin-b did not bind to the lipid layer in the presence of β-Pth. The results provide further insight into the role of hydrophobic and cationic amino acid residues in antimicrobial activity.

KEYWORDS: antimicrobial peptide, puroindoline, purothionin, neutron reflectometry, FTIR spectroscopy, surface pressure

INTRODUCTION

Plants produce proteins and peptides with antimicrobial and antifungal activities as a defense mechanism against pathogenic species, which exert their activity through interaction with the cytoplasmic membrane of the target pathogen.[1,2] In previous studies, we have characterized the lipid membrane interactions of puroindoline (Pin) and purothionin (Pth) proteins (both isolated from hexaploid wheat) using air/liquid monolayer membrane models.[3–5] Pins are ~13 kDa proteins that occur as two wild-type isoforms, Pin-a and Pin-b, which both feature a Trp-rich domain that is thought to be the site of interaction with lipid membranes and has sequence similarity to indolicidin, a mammalian antimicrobial peptide.[6] Pins are up-regulated during times of pathogenic attack and have been shown to act against known plant pathogens including fungal pathogens as well as Gram-positive and Gram-negative bacteria.[7–9]

The Trp-rich domain is not fully conserved between the wild-type isoforms; Pin-a contains five Trp residues (WRWWKWWK), and Pin-b has a truncated domain containing three Trp residues (WPTKWWK).[10,11] Moreover, allelic variation in Pin-b gene expression within certain wheat varieties leads to a mutant form of Pin-b containing a single residue substitution of tryptophan to arginine (Trp-44 to Arg-44) within the Trp-rich domain.[12] This Pin-b mutant domain has the sequence WPTKWRK, and its presence in wheat is associated with the occurrence of hard-textured endosperm, which is a quality determinant for food use.[13,14] Using a combination of surface-sensitive techniques, we have further demonstrated that this single residue substitution reduces depth of penetration into lipid membranes relative to the wild-type Pin-b,[15,16] and we also determined a major effect of this point mutation on the synergistic interactions of Pin-a and Pin-b with respect to lipid membrane penetration.[3]

Pths are of lower molecular mass (~5 kDa) than the Pins and do not feature any Trp residues within their primary structure.[17] Here we focus on β-purothionin (β-Pth), which is believed to interact with lipids via a leucine-rich surface helix.[18] The individual actions of Pths and Pins have been explored in vitro, where it has been established that they have contrasting mechanisms of action.[19] They are co-localized in the wheat seed, which raises the possibility of synergistic or co-operative activity against pathogens. Here we examine interactions of Pin-a, Pin-b (both wild-type and Trp-44 to Arg-44 mutant forms), and β-Pth as mixed and sequentially adsorbed systems with air/liquid lipid monolayer models so that we may test this hypothesis. Surface pressure measurements and external reflection-Fourier transform infrared (ER-FTIR) spectroscopy have been used to monitor the surface penetration and adsorption of mixed/sequential β-Pth/Pin systems to lipid monolayers. Although these techniques cannot differentiate between the different proteins within a system, the combined ability to probe the protein penetration and the lipid layer structure provided a useful insight into the mechanism of interaction of each protein with lipid membranes. In addition, neutron reflectometry (NR) has been employed to study the interfacial layer structure of selected systems.

◼ MATERIALS AND METHODS

Materials. The anionic lipid 1,2-dipalmitoyl-sn-*glycero*-3-phospho-(1′-*rac*-glycerol) (DPPG, synthetic, purity > 99%), was purchased from Avanti Polar Lipids (Alabaster, AL, USA) and used without further purification. Stock solutions (1 mg/mL) of DPPG were prepared in HPLC grade chloroform (Sigma-Aldrich, Dorset, UK) and stored at room temperature. Wild-type Pin-a and Pin-b were extracted from flour milled from Claire winter wheat and purified using Triton X-114 phase partitioning and chromatographic techniques as described previously.[20] β-Pth was purified on a C18 reverse phase HPLC as described previously;[21] the starting material used in this process was the Pth-rich fraction obtained as a byproduct of the purification of Pin-b. The mutant Pin-bs was purified in the same manner but from flour milled from Soissons winter wheat (hence the designation Pin-bs). Mixed protein solutions were prepared at a 1:1 molar ratio to achieve the desired total protein concentration.

Surface Pressure Measurements. Surface pressure measurements were performed using a model 602m PTFE Langmuir trough (Nima Technology Ltd., Coventry, UK) equipped with barriers used for monolayer compression experiments. A paper Wilhelmy plate attached to a surface pressure sensor was used to monitor the surface pressure. Lipid monolayers were made at the air/liquid interface by using a method described previously.[22] Briefly, the trough was filled with 80 mL of 20 mM sodium phosphate buffer (pH 7.0), and DPPG monomolecular layers were compressed and held in a condensed phase at 22 mN/m. The stability of the lipid films was monitored through surface pressure versus time measurements. When the lipid film had stabilized, 1 mL of appropriate protein solution was added to the subphase so that the final concentration of the protein was 0.48 μM. Protein penetration into the lipid layer was then monitored as surface pressure versus time measurements for approximately 120 min before addition of the second protein if sequential protein addition (total protein concentration in trough now at 0.96 μM) was being studied. Protein binding was then monitored by surface pressure leading to a total protein adsorption time of 250 min. Experiments were repeated three times to determine the mean change in surface pressure.

External Reflection FTIR Spectroscopy. ER-FTIR spectra were recorded using a ThermoNicolet Nexus instrument (Madison, WI, USA) fitted with a 19650 series monolayer/grazing angle accessory (Specac, Kent, UK). The instrument was also fitted with a mercury cadmium telluride detector and connected to an air-dryer to purge the instrument of water and carbon dioxide. The accessory was also equipped with a small PTFE trough complete with a barrier used to control lipid compression; the grazing incident angle was aligned at 55° to the surface of the trough. Access to the trough throughout the experiment was via a small sliding lid to maintain the dry air purge. Protein–lipid interactions were analyzed using external reflectance using a method described previously.[22] All FTIR spectra were collected at a resolution 4 cm^{-1}, where 256 interferograms were collected, co-added, and ratioed against a background spectrum of D$_2$O buffer solution.

In each experiment, 9.5 mL of 20 mM sodium phosphate buffer prepared in D$_2$O (pD 7.0) was placed in the trough and a background single-beam spectrum was recorded, allowing time for the sample chamber purge to remove H$_2$O vapor and CO$_2$ from the atmosphere. After recording of a background spectrum, 5 μL of 0.5 mg/mL DPPG was spread onto the surface of the buffer and compressed to 22 mN/m. Sample scans were taken after compression to ensure the stability of the lipid film, which was monitored through the observation of the CH$_2$ symmetric and asymmetric stretching frequencies in the phospholipid tails in the regions of 2854–2850 and 2924–2916 cm^{-1}, respectively. Protein solution (0.5 mL) was injected into the subphase in sequential experiments to make a final protein concentration of 0.48 μM on addition of the first protein and a total subphase protein concentration of 0.96 μM after addition of both proteins. Spectra were continuously collected for the first 15 min after protein injection, and one spectrum was collected every 15 min for the rest of the collection time. Sequential adsorption experiment timing was as described for surface pressure measurements. The interaction of the protein with the lipid monolayer was observed by monitoring the amide I region, 1700–1600 cm^{-1}, and the aforementioned CH$_2$ asymmetric and symmetric stretching frequencies.

To correct for any water vapor present, H$_2$O and HOD spectra were scaled and subtracted against protein adsorbed spectra, the degree of subtraction being dependent on the adsorption time as well as the amount of H/D exchange. The HOD spectra used for scaling and subtraction purposes were collected during the purge of the sample area prior to the addition of the lipid film. No further processing was performed to the data. Experiments were performed in triplicate unless stated otherwise

Neutron Reflectivity (MNR) of Pin-a and B-Pth Synergistic Systems. NR data sets were collected and reduced at SURF and CRISP neutron reflectometers at ISIS (Rutherford Appleton Laboratory, Didcot, UK) using respective Q ranges of 0.01–0.35, which translates to neutron wavelengths of 0.55–6.8 and 0.5–6.5 Å respectively. Neutron scattering is a nuclear effect such that for hydrogen and deuterium the scattering length is significantly different (Table 1), which allows the use of isotopic substitution to produce a

Table 1. Summary of Scattering Length, Scattering Length Density, and Molecular Mass of the Hydrogenated (h) and Deuterated (d) Lipid and Protein Components

lipid/protein	scattering length (10^{-3} Å)	scattering length density (10^{-6}/Å^2)	mol wt (g/mol)
(h) DPPG	0.38	0.36	721
(tail d) DPPG	6.84	6.24	783
DPPG headgroup	6.13	2.52	299
(h) DPPG tail region	−0.32	−0.398	422
(d) DPPG tail region	6.13	7.54	484
Pin-a in NRW	31.13	1.97	12290
β-Pth in NRW	11.19	1.86	4953

number of reflectivity profiles corresponding to a single interfacial structure.[23] In conjunction with NR, this provides a way of identifying the interfacial structure of a multicomponent system. Details of the procedure to obtain and fit protein–lipid profiles have been described previously.[5]

Protein adsorption to DPPG monolayers was measured on a PTFE Langmuir trough as described above for surface pressure measurements. NR profiles were recorded before and after addition of protein, allowing time for equilibrium of the lipid/protein systems. Experiments were carried out on an aqueous subphase composed of air contrast matched water (nonreflective water (NRW): 8% D$_2$O, 92% H$_2$O); this was to make the reflectivity profile sensitive only to material at the air/liquid interface. Data were collected at two angles for experiments on NRW 0.7° and 1.5°; the beam intensity was calibrated with respect to a clean D$_2$O surface. Data were obtained using phospholipids with hydrogenated and deuterated tail regions to provide isotopic contrast between the protein and the phospholipid at the interface.

The raw data from NR experiments were reduced, and data from multiple angles were stitched together at the respective beamline. The reflectivity profiles were then analyzed using optical matrix formalism,[24] to fit Abeles layer models to an interfacial structure using the data-fitting program RasCAL developed at ISIS by Hughes. A typical modeling procedure calculates the reflectivity based on fitting structural parameters: number of layers at the interface, thickness (τ), and scattering length density (ρ) of each layer and layer roughness. A set of reflectivity profiles measured under different isotopic conditions are fitted together to the same parameters except for differences in scattering length density; this allows different components within the system to be highlighted, and the volume fraction (Φ) of each component to be determined.[25]
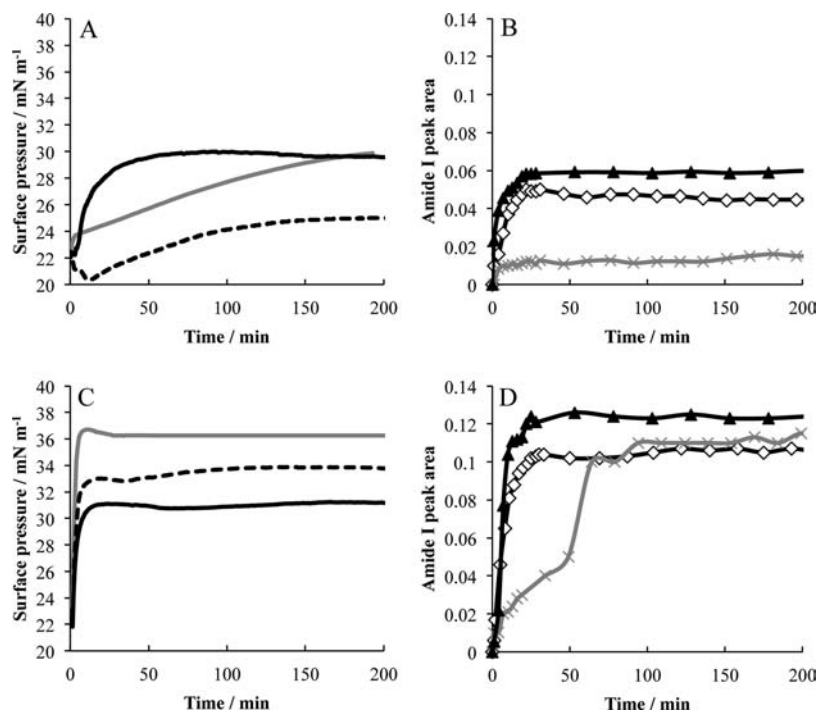
Figure 1. Surface pressure (A, C) and amide I peak areas (B, D) as a function of time for co-binding of β-Pth/Pin-a (black line, triangles), β-Pth/Pin-b (black dotted line, diamonds), and β-Pth/Pin-bs (gray line, crosses) to a DPPG monolayer. Total protein concentration used is 0.48 μM for panels A and B and 0.96 μM for panels C and D.

For each layer within the fit, the scattering length densities of the individual components (Table 1) can be multiplied by their respective volume fractions to give the measured scattering length density for each isotopic contrast reflectivity profile. Thus, the volume fraction of each component within each interfacial layer can be determined. For mixed protein systems, the scattering length density was calculated as the average of Pin-a and β-Pth.[26,27] The surface area and the surface excess are calculated directly from the calculated volume fractions. With knowledge of the volume fraction of each component at the interface, the area per molecule and surface excess can be calculated by assuming that the surface is made of uniform layers.[28]

For the Pin-a/β-Pth systems a three-layer model was needed to provide a suitable fit of the data; this model comprised two layers to describe the tail and head regions of the lipid layer and a third layer showing the presence of protein below the lipid layer. Fitting was constrained to the assumption that the lipid molecules are arranged such that the first lipid layer contains the lipid tails, whereas the second layer contains lipid head groups. Experimental data fitting errors were carried out as described previously using RasCAL's "bootstrap" error analysis function.[5]

■ RESULTS AND DISCUSSION

Co-adsorption of β-Pth and Pin Proteins at an Anionic Lipid Surface. Surface pressure measurements and ER-FTIR spectroscopy were used to probe lipid penetration and the relative mass of protein adsorbed at the lipid interface both in and below the lipid layer.[24] Figure 1 shows surface pressure versus time and amide I peak area versus time for the binding of mixed β-Pth/Pin protein systems to a DPPG condensed monolayer from total protein solution concentrations of 0.48 and 0.96 μM. Values for surface pressure change and amide I peak area are given in Table 2, where the mixed protein systems are compared with values for lipid binding of the individual proteins.

Figure 1A reveals significant differences for each of the 0.48 μM mixed protein systems with respect to the surface pressure

Table 2. Change in Surface Pressure ($\Delta\pi$) and Amide I Peak Areas for Co-adsorption of Puroindolines and β-Pth to a Condensed Phase DPPG Layer

protein concn (μM)	protein mix	$\Delta\pi$ (mN/m)	amide I peak area
0.48	β-Pth	9.5 ± 0.6	0.028 ± 0.006
0.48	Pin-a	7.1 ± 1.0	0.132 ± 0.008
0.48	Pin-b	9.7 ± 0.7	0.095 ± 0.009
0.48	Pin-bs	6.1 ± 0.7	0.105 ± 0.005
0.48	β-Pth/Pin-a	7.3 ± 0.8	0.058 ± 0.008
0.48	β-Pth/Pin-b	3.2 ± 0.3	0.043 ± 0.014
0.48	β-Pth/Pin-bs	7.9 ± 0.7	0.017 ± 0.011
0.96	β-Pth/Pin-a	9.9 ± 0.6	0.135 ± 0.004
0.96	β-Pth/Pin-b	11.3 ± 0.5	0.101 ± 0.017
0.96	β-Pth/Pin-bs	13.7 ± 0.7	0.112 ± 0.009

increase upon binding to the DPPG layer. For the β-Pth/Pin-a mixture, the surface pressure increased over the first 50 min before equilibrating at approximately 29 mN/m, which represented an increase of 7.3 ± 0.8 mN/m. For β-Pth/Pin-bs the increase in surface pressure was equivalent to that for the β-Pth/Pin-a system; however, the rate of increase was slower. The β-Pth/Pin-b mixed system resulted in a significantly lower increase in surface pressure of only 3.2 ± 0.3 mN/m. These results for the mixed protein systems revealed differences in the level of penetration of protein into the lipid layer that could not be directly related to the surface pressure values recorded for Pin proteins binding as single proteins. This particularly relates to the β-Pth/Pin-b mixed system. The surface pressure change for Pin-b penetration was the highest of the three Pin proteins, and binding of β-Pth as a single protein also resulted in a similarly high level of lipid penetration (Table 2). However, for the mixed system there was observed a significant reduction in
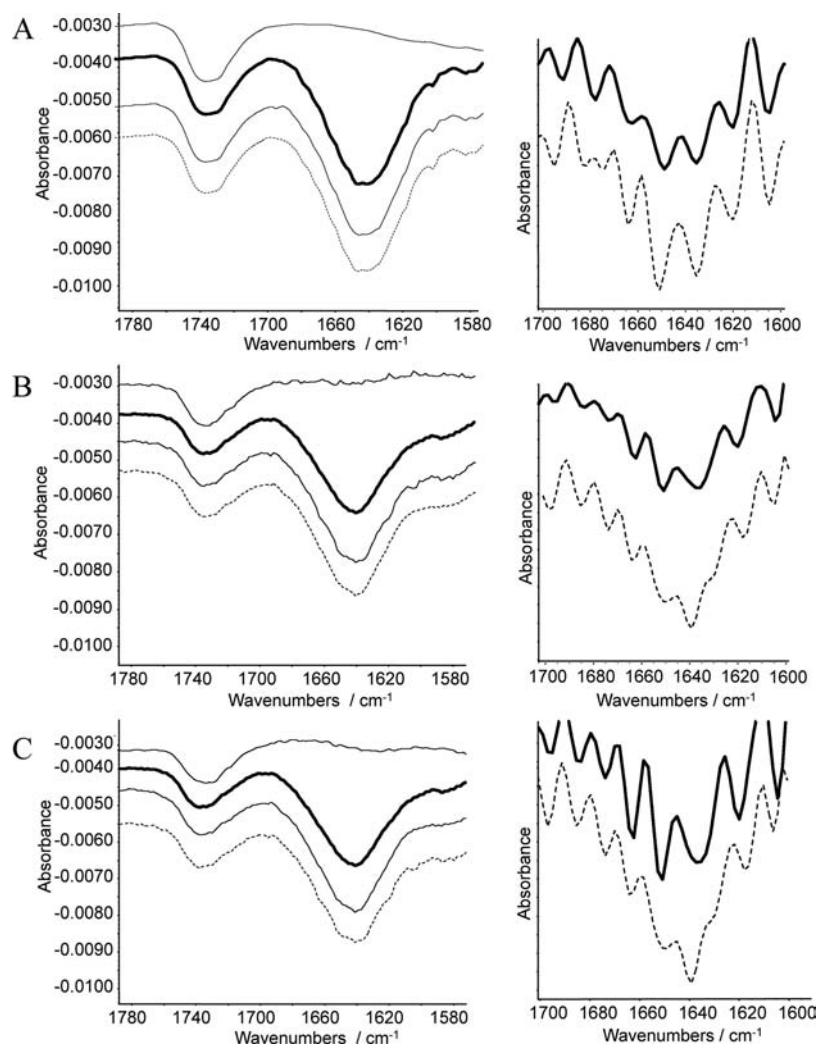
Figure 2. Amide spectral region showing the co-binding of (A) β-Pth/Pin-a, (B) β-Pth/Pin-b, and (C) β-Pth/Pin-bs to the DPPG surface. Spectra are provided for 0, 15, 45, and 60 min after addition of 0.96 μM protein to the lipid subphase and presented offset with increasing adsorption time in descending order. Deconvolution of the amide I peak is also provided for 15 (bold line) and 60 (dashed line) min spectra.

penetration to approximately one-third the level for either of the individual proteins. This could not be ascribed to a concentration effect, because 0.24 μM Pin-b, which equates to the concentration of Pin-b present in the 0.48 μM mixed protein system, results in a surface pressure shift of 9.0 mN/m (data not shown).

The FTIR spectra provided further information about the protein−lipid interactions through changes in the carbonyl and amide I region (1800 and 1550 cm^{-1}) and the hydrocarbon region, particularly the C−H stretch region between 3050 and 2750 cm^{-1}. In the C−H stretch region, the CH$_2$ asymmetric stretch at approximately 2920 cm^{-1} was monitored to investigate formation of the compressed lipid monolayer and the effect of protein addition on the lipid layer structure. Within the carbonyl region, a peak at 1735 cm^{-1} was observed corresponding to the C−O stretch vibration within the lipid headgroup, and a peak at approximately 1650 cm^{-1} was observed corresponding to the protein amide I peak.

For the β-Pth/Pin co-adsorption experiments, no change in the lipid hydrocarbon peaks was observed during protein binding to the lipid surface; however, on addition of protein, the amide I peak was present and its peak area monitored as a function of time. Figure 1B shows the change in the amide I

peak during the adsorption of the 0.48 μM mixed protein systems to the condensed phase DPPG at the air/liquid interface. As observed for the surface pressure data, the FTIR data for the mixed systems does not quantitatively match or fit to a pattern that might be suggested by the behavior of the individual Pin proteins. For example, the amide I peak area change for 0.48 μM β-Pth/Pin-bs suggested a similar level of binding to that of 0.48 μM β-Pth, but not to 0.48 μM Pin-bs (Table 2). This observation, together with the surface pressure data, may suggest some level of competitive adsorption from these mixed system solutions.

At the higher protein concentration of 0.96 μM, differences in adsorption behavior between the β-Pth/Pin systems were less obvious (Table 2). With regard to surface pressure measurements, all protein systems resulted in a rapid increase in surface pressure that reached equilibrium within 10 min, leading to surface pressure changes of 9.9, 11.3, and 13.7 mN/ m for β-Pth/Pin-a, β-Pth/Pin-b, and β-Pth/Pin-bs systems, respectively. The rate of increase in surface pressure was similar to that measured for β-Pth binding alone.[5] FTIR data showed a rapid appearance and then increase in the amide I peak area for adsorption of β-Pth/Pin-a and β-Pth/Pin-b to the lipid surface. As shown in Table 2, the peak area increased to values similar
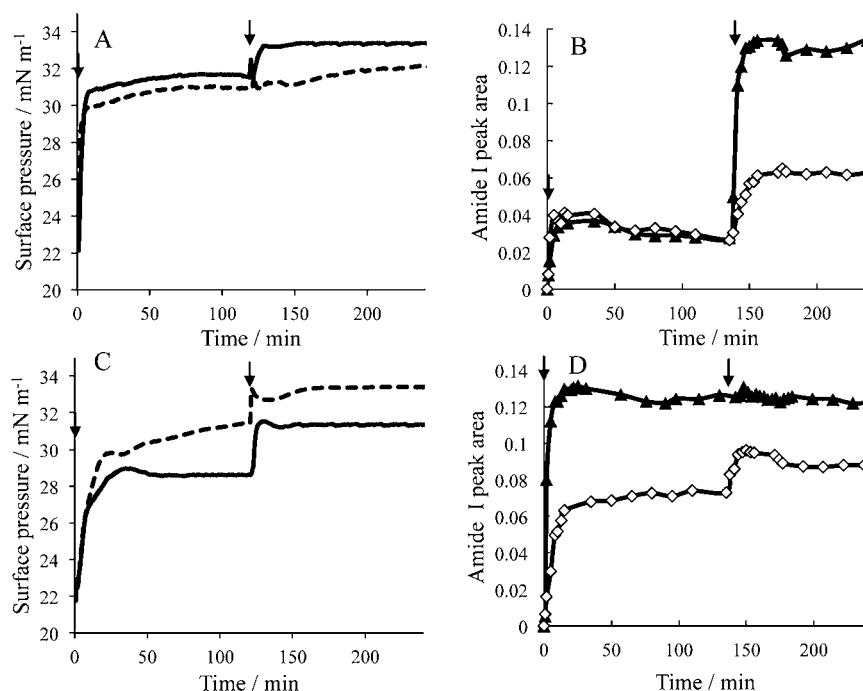
Figure 3. Surface pressure (A, C) and amide I peak areas (B, D) as a function of time for sequential adsorption of proteins to a DPPG monolayer. Panels A and B show adsorption of 0.48 μM β-Pth followed by 0.48 μM Pin-a (solid black line or triangles) or 0.48 μM Pin-b (dotted black line or diamonds). Panels C and D show adsorption of 0.48 μM Pin-a (solid black line or triangles) or 0.48 μM Pin-b (dotted black line or diamonds) followed by 0.48 μM β-Pth. The arrows indicate the time points for addition of protein to the subphase. The total protein concentration added for each experiment was 0.96 μM.

to those observed for the single-protein Pin systems at a concentration of 0.48 μM. For β-Pth/Pin-bs, the FTIR peak area isotherm is different, showing two rates of adsorption: an initial rapid increase (to a peak area of approximately 0.05) that begins to plateau before a second increase in peak area at approximately 50 min to reach equilibrium. The final peak area was similar to that of the Pin-bs only system. This appears to suggest initial adsorption or penetration of the smaller β-Pth before blanket-like adsorption of Pin-bs. Thus, at the higher protein concentration (0.96 μM) of the mixed system, Pin-bs was more competitive compared to binding at lower concentrations (0.48 μM) where β-Pth dominated.

These results show protein concentration dependence of the competitive binding behavior to the lipid surface, particularly for systems involving Pin-b and Pin-bs. For Pin-a, adsorption reaches values similar to 0.48 μM Pin-a only for the mixed β-Pth/Pin-a (0.48/0.48 μM) sample; however, penetration, as seen by surface pressure measurements, is greater and more like that seen for 0.48 μM β-Pth. β-Pth/Pin-b shows depressed levels of penetration and binding at the lower concentration. However, when the concentration is increased, both the levels of lipid penetration and adsorption of protein below the film are enhanced relative to the individual proteins. Similarly, Pin-bs was shown to compete with β-Pth rather poorly at lower concentration compared to when the total protein concentration is increased.

For the FTIR adsorption experiments, differences in the shape of the amide I peaks provided information on the dominant secondary structure of the adsorbed protein and the lipid surface. Figure 2 shows the carbonyl region of the spectra for the co-adsorption of each mixed protein system at 0.96 μM and also shows deconvolution of the amide I peak. The deconvoluted amide I peaks of the three Pin proteins have been

reported previously,[3,16] whereas others have reported that β-Pth has a high helical content in contact with lipid.[29] For each of the protein systems, β-Pth/Pin-a, β-Pth/Pin-b, and β-Pth/Pin-bs, the amide I peak shape after 15 min of adsorption was similar, showing a symmetrical peak centered at approximately 1644 cm^{-1}. Deconvolution of these peaks enables contributions of different secondary structure environments to be compared between the spectra and shows a split in the amide I peak that suggests some β-sheet content (at approximately 1680 and 1620 cm^{-1}), high helix content (1655 cm^{-1}), and random coil (1640 cm^{-1}). The deconvoluted spectra show that upon adsorption reaching equilibrium, after 60 min, the random coil content of the adsorbed protein layer dominates for the β-Pth/Pin-b and β-Pth/Pin-bs systems but not for β-Pth/Pin-a. This can also be observed in the raw spectra, where the peak maximum shifts toward 1640 cm^{-1} during lipid binding. From our knowledge of the secondary structure of these proteins, this shift toward higher random coil structure would be consistent with an increase in the amount of Pin-b or Pin-bs at the interface. Indeed, the deconvoluted spectra of β-Pth/Pin-b and β-Pth/Pin-bs after 60 min of adsorption are remarkably similar to those observed for Pin-b and Pin-bs alone.[16] According to our previous studies, Pin-a appears to have a higher helix content compared to Pin-b in the presence of lipid and, therefore, less change would be expected for competitive adsorption between Pin-a and β-Pth.[3]

Sequential Protein Adsorption to an Anionic Lipid Surface. Co-adsorption experiments provided evidence of a competitive nature to protein binding to the lipid surfaces. However, if one protein was associated with the lipid first, would this affect the lipid binding behavior of subsequent adsorption of a second protein? To answer this, experiments have been carried out on sequential protein adsorption

Table 3. Change in Surface Pressure ($\Delta\pi$) during Sequential Protein Addition to Condensed Phase DPPG Monolayers

sequential adsorption of	first protein $\Delta\pi$ (mN/m)	second protein $\Delta\pi$ (mN/m)	total $\Delta\pi$ (mN/m)
0.48 μM β-Pth then 0.48 μM Pin-a	9.5 ± 0.6	1.6 ± 0.3	11.1 ± 0.4
0.48 μM Pin-a then 0.48 μM β-Pth	7.9 ± 1	1.5 ± 1	9.3 ± 0.3
0.48 μM β-Pth then 0.48 μM Pin-b	9.0 ± 0.8	0.4 ± 0.3	9.4 ± 0.5
0.48 μM Pin-b then 0.48 μM β-Pth	9.2 ± 0.7	1 ± 0.6	10.2 ± 0.6

experiments of β-Pth and Pins to a condensed DPPG monolayer at the air−liquid interface. The surface pressure profiles and amide I peak areas are shown in Figure 3; values for surface pressure change upon protein addition to the condensed lipid layer are given in Table 3 and those for amide I peak areas in Table 4.

Table 4. Change in ER-FTIR Amide I Peak Area during Sequential Protein Addition to Condensed Phase DPPG Monolayers

sequential adsorption of	amide I peak area after addition of first protein	amide I peak area after addition of second protein
0.48 μM β-Pth then 0.48 μM Pin-a	0.028 ± 0.005	0.128 ± 0.009
0.48 μM Pin-a then 0.48 μM β-Pth	0.132 ± 0.012	0.135 ± 0.013
0.48 μM β-Pth then 0.48 μM Pin-b	0.028 ± 0.005	0.075 ± 0.011
0.48 μM Pin-b then 0.48 μM β-Pth	0.075 ± 0.013	0.093 ± 0.009

In Figure 3A, 0.48 μM β-Pth was added to the buffer subphase and the surface pressure monitored for approximately 120 min before addition of 0.48 μM of either Pin-a or Pin-b. Figure 3C shows the surface pressure profiles for sequential adsorption where the Pin protein is added first. From Figure 3A it can be observed that upon addition of β-Pth to the subphase

there was a rapid increase in the surface pressure within the subsequent 10 min. The system had fully equilibrated to give an increase of 9.5 ± 0.6 mN/m before the addition of the second protein after 120 min (Pin-a or Pin-b). Upon addition of Pin-a to a preadsorbed β-Pth system, the surface pressure quickly increased by 1.6 ± 0.3 mN/m within 30 min and then equilibrated; the total surface pressure change of the complete system was 11.1 ± 0.4 mN/m. When Pin-b was added to a preadsorbed β-Pth system, there was a negligible increase in surface pressure, with a total surface pressure change for the complete β-Pth/Pin-b system of 9.4 ± 0.5 mN/m as compared to 9.0 ± 0.8 mN/m for β-Pth alone.

When the order of the protein addition is reversed, Pin-a and Pin-b show slower kinetics toward equilibrium binding than those for β-Pth, giving surface pressure increases of 7.9 ± 1.0 and 9.2 ± 0.7 mN/m after 120 min, respectively, as has been observed in previous work.[5,16] On the addition of β-Pth to a preadsorbed Pin-a system, there was a rapid increase in surface pressure, equilibrating at a total surface pressure change for adsorption of both proteins (total protein concentration of 0.96 μM) at 9.3 ± 0.3 mN/m. This total surface pressure change is similar to the surface pressure change for the 0.48 μM β-Pth single-protein system on this trough (Figure 3A). When β-Pth was added to a preadsorbed Pin-b/DPPG layer, a small increase
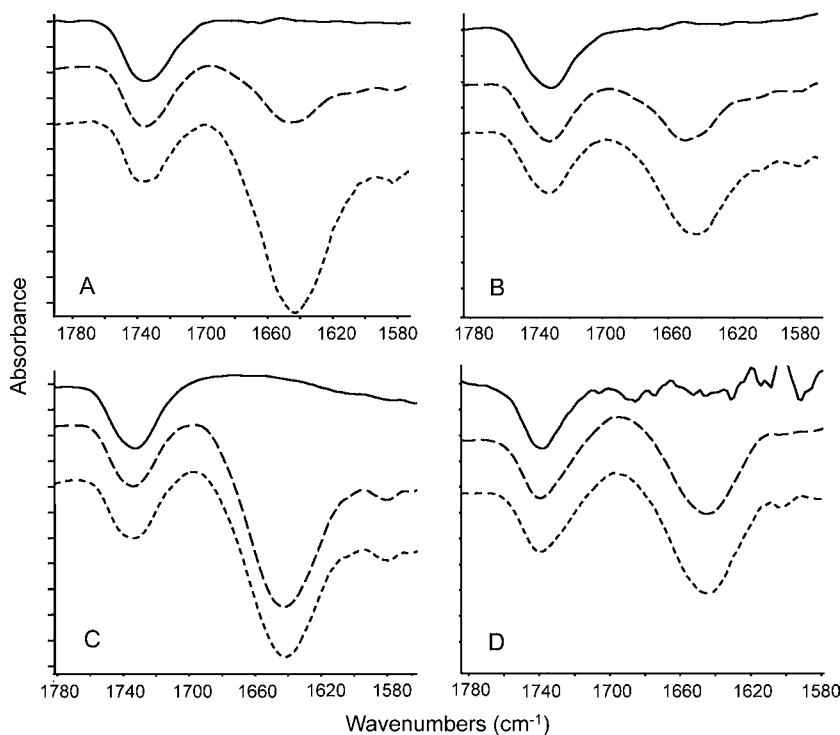
Figure 4. Amide I spectra showing the sequential adsorption to DPPG monolayer for β-Pth followed by Pin-a (a) and Pin-b (b) and Pin-a (c) or Pin-b (d) addition followed by β-Pth. Each panel shows three spectra: before protein addition (top), 130 min after addition of first protein (middle), and approximately 100 min after addition of the second protein (bottom).
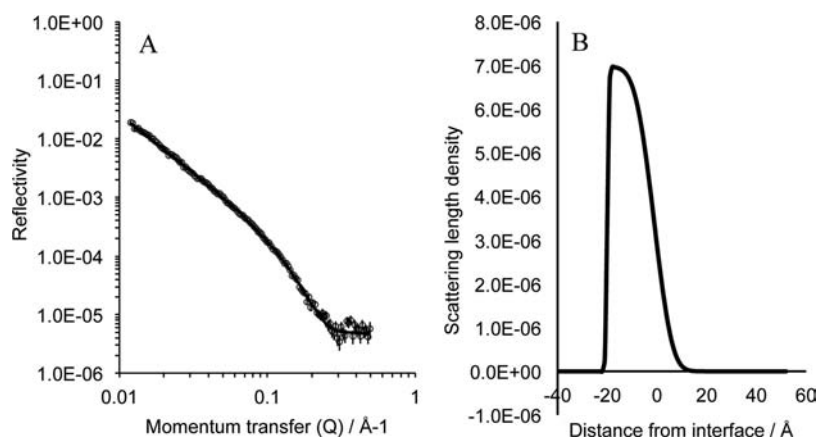
Figure 5. (A) Neutron reflectivity profile for chain-deuterated DPPG at the air/water interface showing best two-layer model-to-data fit as the solid line. (B) Scattering length density profile as a function of distance from interface as determined from the fit. The corresponding fit parameters are provided in Table 5.

was observed, giving a total pressure change for both proteins of 10.2 ± 0.6 mN/m.

Comparison of the surface pressure changes for these sequential adsorption systems shows similar total surface pressure changes after adsorption of the two proteins between all systems, ranging from 9.3 to 11.1 mN/m, and using the Bonferroni multiple comparison ($P < 0.05$) statistical test there are no significant differences between the different systems when the Pins were added first; however, the changes are significant when β-Pth is added to the subphase first followed by Pin-a. Furthermore, there are differences in the step changes on addition of the second protein, highlighting differences in the ability of the individual proteins to penetrate into the lipid layer. Because surface pressure changes are sensitive to penetration of protein into the lipid layer, a limit in the maximum increase in surface tension at high protein concentration might be expected upon full compression of the lipid layer.

The amide I peak areas from the ER-FTIR experiments for these sequential adsorption systems are shown in Figure 3B,D. The associated spectra showing the carbonyl region both prior to addition of protein and after adsorption equilibrium of each sequentially adsorbed protein are given in Figure 4. Figure 3B compares the two sequential systems when β-Pth was added to the lipid subphase first and Pin-a or Pin-b was added second. Upon β-Pth addition, adsorption of protein was observed by the rapid appearance of a peak in the amide I region to produce a peak maximum at 1644 cm^{-1}; the system was fully equilibrated within 10 min after protein addition. Upon the addition of Pin-a to the β-Pth/lipid system, the size of the amide I peak increased 4-fold within 10 min and the system fully equilibrated within an hour with a peak maximum at 1643 cm^{-1}. Addition of Pin-b to the β-Pth adsorbed lipid surface resulted in a 2-fold increase in the amide I peak area and a shift in the peak maximum to 1640 cm^{-1}. The corresponding final peak area values are given in Table 4.

When the order of protein addition was reversed, the addition of Pin-a to the DPPG layer was accompanied by the appearance of a strong peak in the amide I region with a peak maximum at 1644 cm^{-1} (Figures 3B and 4). According to the differences observed in the amide I peak areas, the amount of Pin-a adsorbed at 0.48 μM was approximately 4 times that of β-Pth to DPPG and equivalent to the total protein adsorption (at 0.96 μM) for β-Pth/Pin-a sequential adsorption. This can be

seen from comparison of peak area data in Tables 2 and 4. Addition of β-Pth to the Pin-a/DPPG surface resulted in no further increase in adsorbed amount according to the amide I peak area.

When Pin-b is added to the subphase first (Figure 3D), the amide I peak area reaches a value of approximately 0.075 at equilibrium; this value is approximately half that observed for adsorption of Pin-a and equivalent to the value seen for the total adsorption of the β-Pth/Pin-b sequential system. Addition of β-Pth to the Pin-b/lipid surface led to an increase in the amide I peak area from 0.075 to 0.93, resulting in a final amide I peak area that was 30% greater than the total amide I peak area observed when β-Pth was adsorbed to the lipid layer first.

With regard to the impact that the protein binding has on lipid structure, our data (not shown) support previous findings,[5] with an ~8% reduction in CH$_2$ asymmetric peak area upon β-Pth addition. However, this occurs only in cases when β-Pth is adsorbed first. If added to a preadsorbed Pin/lipid surface, the purothionin is not able to disrupt the lipid surface. Thus, the mechanism of lipid removal as suggested in the literature is prevented or reduced in the presence of puroindolines.[19,30]

For the 0.96 μM Pin-b/β-Pth system, the amide I peak maximum shifted toward 1640 cm^{-1} during adsorption, suggesting a change in secondary structure of the adsorbed protein toward an increase in random coil, seen from deconvolution of the amide I peak. The observed shift in the amide I peak appears to link with an increase in the amount of random coil correlating with an increase in the amount of Pin-b at the interface.[3,16] Clearly, the adsorption here is competitive, with Pin-b appearing to dominate at equilibrium. This finding is reflected when the proteins are added sequentially to the lipid, where we see evidence of greater adsorption (amide I peak area) and penetration (surface pressure change) of protein into lipid when Pin-b is added first. If β-Pth is first, these values are reduced compared to when the proteins are co-adsorbed.

NR Analysis of the Protein–Lipid Layer Structure for the Co-adsorbed Protein Systems. To determine the protein–lipid layer structure for protein binding to the lipid monolayer, neutron reflectivity studies have been carried out to compare the lipid binding behavior of the β-Pth/Pin-a co-adsorbed and sequential binding systems. This enabled us to confirm levels of penetration compared to binding and

Table 5. NR Fit Parameters for Pin-a/β-Pth Binding to DPPG

layer + H/D contrast	fit parameters		Φ_{lipid}	$\Phi_{protein}$	A_{lipid} (Å^2)	Γ_{prot} (mg/m^2)
	τ (Å)	ρ (10^{-6}/Å^2)				
DPPG Only						
layer 1						
d-DPPG on NRW	16.4	6.9	0.91		54.1	
layer 2						
d-DPPG on NRW	6.3	2.3	0.91		49.3	
0.96 μM Pin-a/β-Pth Co-adsorbed to DPPG						
layer 1						
d-DPPG on NRW	17.3	6.4	0.81	0.16	58.2	0.32
h-DPPG on NRW	17.3	−0.01				
layer 2						
d-DPPG on NRW	8	1.79	0.61	0.13	58.2	0.14
h-DPPG on NRW	8	1.79				
layer 3						
d-DPPG on NRW	37	0.7		0.36		1.72
h-DPPG on NRW	37	0.7				
0.48 μM β-Pth Adsorbed to 0.48 μM Pin-a and DPPG						
layer 1						
d-DPPG on NRW	20	4.1	0.5	0.16	81.0	0.45
h-DPPG on NRW	20	0.15				
layer 2						
d-DPPG on NRW	10	1.65	0.39	0.35	81.0	0.51
h-DPPG on NRW	10	1.65				
layer 3						
d-DPPG on NRW	34	0.8		0.41		1.81
h-DPPG on NRW	34	0.8				

adsorption below the lipid layer and to compare with the pure protein adsorption studies reported previously.[5]

Figure 5A shows the NR profile and the best NR model to data fit obtained from a monolayer of tail-deuterated DPPG at the air/liquid interface compressed to 22 mN/m on a NRW subphase. The scattering length density profile across the interface that is described by the fit is shown in Figure 5B, and the structural parameters obtained from these fits are given in Table 5. The phospholipid layer was fitted to a two-layer model, where thicknesses of the lipid acyl region and lipid headgroup were 16.4 and 6.3 Å, respectively. A volume fraction ($\Phi_{lipid\,acyl}$) of 0.91 was calculated for the DPPG acyl chain in the condensed phase with an area per molecule of 54.1 Å^2.

Figure 6A shows the NR profiles and the best three-layer fit obtained for Pin-a/β-Pth co-adsorbed (0.96 μM) to a condensed phase DPPG monolayer; the scattering length density profile of the fit is shown in Figure 6B, and the resulting structural parameters obtained are given in Table 5. The best model-to-data fit used a three-layer interfacial structure, where layers 1 and 2 represented the lipid acyl chain and the headgroup regions of the phospholipid, respectively, and layer 3 represented the protein in the subphase below the lipid layer. The layers were found to be 17.3, 8, and 37 Å, respectively. Protein was found to have penetrated the lipid layer and uniformly distributed within the acyl and lipid headgroup regions ($\Phi_{protein}$ = 0.16 and 0.13, respectively). The protein volume fraction below the lipid layer was found to be 0.36. Calculation of the protein surface excess showed a total amount of protein of 2.18 mg/m^2, where 78% (1.72 mg/m^2) was found underneath the lipid layer and 14% (0.32 mg/m^2) was found in the acyl region. The protein surface excess and the thickness of the protein layer showed similarities with the values previously observed when Pin-a at 0.48 μM was adsorbed to DPPG

alone,[5] both showing a protein layer thickness of approximately 34 Å and similar amounts of total protein surface excess (Table 5). The main differences observed were greater penetration of protein into the acyl region of the lipid and a reduced amount of protein within the headgroup region for the β-Pth/Pin-a system, signifying a difference in the depth of penetration of protein into the lipid as a result of the presence of β-Pth. Previous studies showing the binding of β-Pth to DPPG at 0.48 μM showed penetration into the acyl lipid region to be 0.6 mg/m^2, with 0.31 mg/m^2 within the headgroup and only 0.36 mg/m^2 within a 9 Å region below the lipid layer.[5]

Panels C and D of Figure 6 show the NR profile, the best three-layer fit, and the resulting scattering length density profile for the sequential protein adsorption experiments where 0.48 μM β-Pth is adsorbed to a DPPG surface with preadsorbed Pin-a (0.48 μM). The structural parameters for the three-layer fit are shown in Table 5. As with the co-adsorbed film, the best model-to-data fit obtained for the sequential addition of β-Pth adsorbed to a Pin-a/DPPG surface was a three-layer interfacial structure with layer thicknesses of 20, 10, and 34 Å for the lipid acyl chain, lipid headgroup, and protein below the film, respectively. The volume fraction of lipid was shown to decrease on addition of protein to the lipid surface due to an increase in lipid layer thickness from 22.7 to 30 Å. The layer before the addition of β-Pth was a Pin-a/DPPG layer that has been described previously as having a lipid layer thickness of 26 Å and a protein layer below the lipid of 33.5 Å; the distribution of protein between these layers was 0.2, 0.51, and 1.55 mg/m^2, respectively.[5] Table 5 shows that on addition of 0.48 μM β-Pth to this system, the lipid layer became thicker and the amount of protein within the acyl lipid region and below the lipid layer increased by 0.25 and 0.26 mg/m^2, respectively.
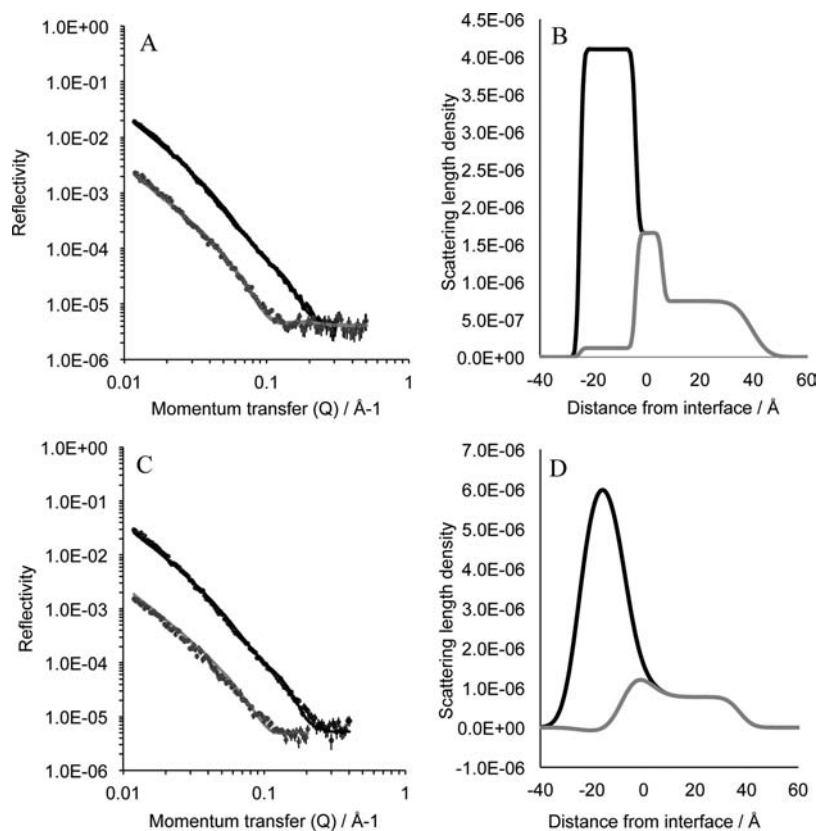
Figure 6. (A) Neutron reflectivity profile for chain-deuterated and hydrogenated DPPG with co-adsorbed 0.48 μM β-Pth/Pin-a showing best two-layer model-to-data fit (gray line for h-lipid contrast and black line for d-lipid contrast). (B) Corresponding scattering length density profile as a function of distance from interface. (C) Neutron reflectivity profile for chain-deuterated and hydrogenated DPPG with sequential adsorbed 0.96 μM total concentration β-Pth/Pin-a showing best two-layer model-to-data fit (gray line for h-lipid contrast and black line for d-lipid contrast). (D) Corresponding scattering length density profile as a function of distance from interface.

The NR data support the findings from FTIR experiments that showed Pin-a as the dominant protein adsorbed from mixed β-Pth/Pin-a systems. However, the presence of a preadsorbed Pin-a layer does not prevent a small increase in surface pressure on addition of β-Pth (1.6 ± 1 mN/m), which was indicative of additional penetration of protein into the lipid. This was confirmed by NR where sequential addition of β-Pth to a Pin-a/lipid surface resulted in increased protein within the lipid head and tail regions and an increased thickness of the lipid layer from 23 Å for the pure lipid layer to 26−27 Å after addition of Pin-a or a mixed Pin-a/β-Pth solution to 30Å after sequential adsorption of the two proteins. Although lipid penetration was enhanced compared to Pin-a only, NR data of the mixed and sequential adsorbed Pin-a/β-Pth systems showed less penetration into the lipid tail region to that seen for lipid binding of β-Pth only,[5] showing that Pin-a has apparently hindered the lipid penetrative behavior of β-Pth.

Competitive Binding between β-Pth and Pins. We have examined the possibility of a synergistic mechanism of interaction of the proteins β-Pth and Pins with respect to their lipid binding properties. However, data have not shown evidence of strong synergy in binding behavior when the presence of the two proteins might lead to enhanced lipid binding. Indeed, competitive binding behavior and differences in the mode of lipid binding of the two types of proteins have been observed.

FTIR and NR measurements from this study and previous studies have shown that the Pins form a thick protein layer

below the lipid surface of approximately 35 Å.[5,15,16] In contrast, the total adsorbed amount for β-Pth is much less as shown by the peak area of the amide I peak by FTIR and in previous studies by NR measurements.[5] However, the relatively small size (5 kDa) and helical amphipathic structure of β-Pth enables it to more rapidly penetrate into the lipid layer. It is less hydrophobic than any of the Pins, but highly cationic with a charge of +8 at pH 7.

The lipid binding Trp-rich loop of the different Pin proteins differs by the number of Trp residues, but the Pins have similarities in MW, hydrophobicity, and isoelectric points. Pin-a has a pI of 10 and Pin-b has a pI of 11 according to 2D electrophoresis studies.[31] However, Pin-b is recognized to be more water-soluble than Pin-a and less inclined to self-associate in aqueous solution;[32] at pH 7 its net charge is +9 compared to +6 for Pin-a. The difference in behavior of the Pin proteins appears to be associated with the Trp-rich loop, rather than total charge or hydrophobicity of the proteins; however, the behavior is not simply linked to number of Trp or cationic residues in this loop. Pin-b is the more penetrative in terms of lipid binding of the Pins with three Trp residues within the loop, compared to five for Pin-a and two for Pin-bs. However, it does have two proline residues within the loop and fewer charged residues within that region, which may promote deeper penetration into the hydrophobic region of the lipid layer, thus behaving most like β-Pth in terms of lipid penetration. Both Pin-a and Pin-bs adsorb strongly to the lipid headgroup region and penetrate less into the lipid tail region of the lipid layer.

Pin-a, however, competes very well with β-Pth and appears to dominate at the lipid surface, whereas Pin-bs competes very poorly and is prevented from binding strongly to the lipid in the presence of β-Pth.

Substituting Pin-b for Pin-bs results in significant differences in the lipid binding behavior of the mixed protein systems studied here and highlights the impact of the amino acid sequence within the Trp-rich loop. The difference between the proteins is a point mutation substitution of Trp to Arg that alters the Trp-rich domain sequence from WPTKWWK for Pin-b to WPTKWRK for Pin-bs. This Trp to Arg substitution has been shown previously to reduce the lipid penetrative ability of the protein while enhancing association below the lipid film, through interaction with the headgroup of the lipid.[15] Upon co-adsorption of Pin-bs with β-Pth, β-Pth dominated at low protein concentrations and prevented binding of Pin-bs. β-Pth also dominated initially over Pin-bs at the higher concentration studied (0.96 μM), as evidenced by a two-step adsorption profile (Figure 1D). However, Pin-b and Pin-bs were shown to dominate lipid binding at equilibrium at high concentration (0.96 μM) as observed from the changes to the FTIR amide I peak during adsorption (Figure 2).

The poor ability of Pin-bs to compete with β-Pth especially at low concentrations is particularly interesting and, when compared to Pin-b, highlights the importance of the hydrophobicity of the lipid binding region of the protein. The findings also link to our previous studies where the co-binding of Pin-a and Pin-b to lipids was investigated and revealed reductions in lipid penetration and binding when Pin-bs was substituted for Pin-b.[3] The result supports the hypothesis that Pin function within wheat endosperm is lipid mediated.[33] In addition, the different lipid binding behaviors of these proteins provide further insight into the impact of hydrophobic and cationic amino acids on the functional properties of antimicrobial peptides and proteins.

■ AUTHOR INFORMATION

Corresponding Author

*(R.J.G.) Phone: +44-118-3788446. E-mail: rebecca.green@reading.ac.uk.

Notes

The authors declare no competing financial interest.

■ REFERENCES

(1) Bowles, D. J. Defense-related proteins in higher plants. *Annu. Rev. Biochem.* **1990**, *59*, 873−907.

(2) Broekaert, W. F.; Cammue, B. P. A.; De Bolle, M. F. C.; Thevissen, K.; De Samblanx, G. W.; Osborn, R. W.; Nielson, K. Antimicrobial peptides from plants. *Crit. Rev. Plant Sci.* **1997**, *16*, 297−323.

(3) Clifton, L. A.; Green, R. J.; Frazier, R. A. Puroindoline-b mutations control the lipid binding interactions in mixed puroindoline-a:puroindoline-b systems. *Biochemistry* **2007**, *46*, 13929−13937.

(4) Clifton, L. A.; Sanders, M.; Kinane, C.; Arnold, T.; Edler, K. J.; Neylon, C.; Green, R. J.; Frazier, R. A. The role of protein hydrophobicity in thionin-phospholipid interactions: a comparison of α1 and α2-purothionin adsorbed anionic phospholipid monolayers. *Phys. Chem. Chem. Phys.* **2012**, *14*, 13569−13579.

(5) Clifton, L. A.; Sanders, M. R.; Hughes, A. V.; Neylon, C.; Frazier, R. A.; Green, R. J. Lipid binding interactions of antimicrobial plant seed defence proteins: puroindoline-a and β-purothionin. *Phys. Chem. Chem. Phys.* **2011**, *13*, 17153−17162.

(6) Petersen, F. N. R.; Jensen, M. O.; Nielsen, C. H. Interfacial tryptophan residues: a role for the cation-pi effect? *Biophys. J.* **2005**, *89*, 3985−3996.

(7) Capparelli, R.; Palumbo, D.; Iannaccone, M.; Ventimiglia, I.; Di Salle, E.; Capuano, F.; Salvatore, P.; Amoroso, M. G. Cloning and expression of two plant proteins: similar antimicrobial activity of native and recombinant form. *Biotechnol. Lett.* **2006**, *28*, 943−949.

(8) Jing, W. G.; Demcoe, A. R.; Vogel, H. J. Conformation of a bactericidal domain of puroindoline a: structure and mechanism of action of a 13-residue antimicrobial peptide. *J. Bacteriol.* **2003**, *185*, 4938−4947.

(9) Dubreil, L.; Gaborit, T.; Bouchet, B.; Gallant, D. J.; Broekaert, W. F.; Quillien, L.; Marion, D. Spatial and temporal distribution of the major isoforms of puroindolines (puroindoline-a and puroindoline-b) and non specific lipid transfer protein (ns-LTPle(1)) of *Triticum aestivum* seeds. Relationships with their *in vitro* antifungal properties. *Plant Sci.* **1998**, *138*, 121−135.

(10) Bhave, M.; Morris, C. F. Molecular genetics of puroindolines and related genes: regulation of expression, membrane binding properties and applications. *Plant Mol. Biol.* **2008**, *66*, 221−231.

(11) Lillemo, M.; Simeone, M. C.; Morris, C. F. Analysis of puroindoline a and b sequences from *Triticum aestivum* cv. 'Penawawa' and related diploid taxa. *Euphytica* **2002**, *126*, 321−331.

(12) Martin, J. M.; Frohberg, R. C.; Morris, C. F.; Talbert, L. E.; Giroux, M. J. Milling and bread baking traits associated with puroindoline sequence type in hard red spring wheat. *Crop Sci.* **2001**, *41*, 228−234.

(13) Martin, J. M.; Meyer, F. D.; Morris, C. F.; Giroux, M. J. Pilot scale milling characteristics of transgenic isolines of a hard wheat over-expressing puroindolines. *Crop Sci.* **2007**, *47*, 497−506.

(14) Morris, C. F.; Lillemo, M.; Simeone, M. C.; Giroux, M. J.; Babb, S. L.; Kidwell, K. K. Prevalence of puroindoline grain hardness genotypes among historically significant North American spring and winter wheats. *Crop Sci.* **2001**, *41*, 218−228.

(15) Clifton, L. A.; Green, R. J.; Hughes, A. V.; Frazier, R. A. Interfacial structure of wild-type and mutant forms of puroindoline-b bound to DPPG monolayers. *J. Phys. Chem. B* **2008**, *112*, 15907−15913.

(16) Clifton, L. A.; Lad, M. D.; Green, R. J.; Frazier, R. A. Single amino acid substitutions in puroindoline-b mutants influence lipid binding properties. *Biochemistry* **2007**, *46*, 2260−2266.

(17) Clore, G. M.; Nilges, M.; Sukumaran, D. K.; Brunger, A. T.; Karplus, M.; Gronenborn, A. M. The 3-dimensional structure of α-1-purothionin in solution − combined use of nuclear-magnetic-resonance, distance geometry and restrained molecular dynamics. *EMBO J.* **1986**, *5*, 2729−2735.

(18) Hughes, P.; Dennis, E.; Whitecross, M.; Llewellyn, D.; Gage, P. The cytotoxic plant protein, β-purothionin, forms ion channels in lipid membranes. *J. Biol. Chem.* **2000**, *275*, 823−827.

(19) Llanos, P.; Henriquez, M.; Minic, J.; Elmorjani, K.; Marion, D.; Riquelme, G.; Molgo, J.; Benoit, E. Puroindoline-a and α1-purothionin form ion channels in giant liposomes but exert different toxic actions on murine cells. *FEBS J.* **2006**, *273*, 1710−1722.

(20) Day, L.; Bhandari, D. G.; Greenwell, P.; Leonard, S. A.; Schofield, J. D. Characterization of wheat puroindoline proteins. *FEBS J.* **2006**, *273*, 5358−5373.

(21) Jones, B. L.; Lookhart, G. L.; Johnson, D. E. Improved separation and toxicity analysis methods for purothionins. *Cereal Chem.* **1985**, *62*, 327−331.

(22) Lad, M. D.; Birembaut, F.; Clifton, L. A.; Frazier, R. A.; Webster, J. R. P.; Green, R. J. Antimicrobial peptide-lipid binding interactions and binding selectivity. *Biophys. J.* **2007**, *92*, 3575−3586.

(23) Green, R. J.; Su, T. J.; Lu, J. R.; Webster, J. R. P. The displacement of preadsorbed protein with a cationic surfactant at the hydrophilic SiO_2–water interface. *J. Phys. Chem. B* **2001**, *105*, 9331–9338.

(24) Wolf, M. B. A. E. *Principles of Optics*, 6th ed.; Pergamon Press: Oxford, UK, 1984.

(25) Penfold, J.; Richardson, R. M.; Zarbakhsh, A.; Webster, J. R. P.; Bucknall, D. G.; Rennie, A. R.; Jones, R. A. L.; Cosgrove, T.; Thomas, R. K.; Higgins, J. S.; Fletcher, P. D. I.; Dickinson, E.; Roser, S. J.; McLure, I. A.; Hillman, A. R.; Richards, R. W.; Staples, E. J.; Burgess, A. N.; Simister, E. A.; White, J. W. Recent advances in the study of chemical surfaces and interfaces by specular neutron reflection. *J. Chem. Soc., Faraday Trans.* **1997**, *93*, 3899–3917.

(26) Thomas, R. K. Neutron reflection from liquid interfaces. *Annu. Rev. Phys. Chem.* **2004**, *55*, 391–426.

(27) Penfold, J.; Staples, E.; Thompson, L.; Tucker, I. The composition of nonionic surfactant mixtures at the air/water interface as determined by neutron reflectivity. *Colloid Surf. A–Physicochem. Eng. Asp.* **1995**, *102*, 127–132.

(28) Lu, J. R.; Lee, E. M.; Thomas, R. K. The analysis and interpretation of neutron and X-ray specular reflection. *Acta Crystallogr. A* **1996**, *52*, 11–41.

(29) Richard, J. A.; Kelly, I.; Marion, D.; Auger, M.; Pezolet, M. Structure of β-purothionin in membranes: a two-dimensional infrared correlation spectroscopy study. *Biochemistry* **2005**, *44*, 52–61.

(30) Mattei, C.; Elmorjani, K.; Molgo, J.; Marion, D.; Benoit, E. The wheat proteins puroindoline-a and α1-purothionin induce nodal swelling in myelinated axons. *Neuroreport* **1998**, *9*, 3803–3807.

(31) Branlard, G.; Amiour, N.; Igrejas, G.; Gaborit, T.; Herbette, S.; Dardevet, M.; Marion, D. Diversity of puroindolines as revealed by two-dimensional electrophoresis. *Proteomics* **2003**, *3*, 168–174.

(32) Clifton, L. A.; Sanders, M. R.; Castelletto, V.; Rogers, S. E.; Heenan, R. K.; Neylon, C.; Frazier, R. A.; Green, R. J. Puroindoline-a, a lipid binding protein from common wheat, spontaneously forms prolate protein micelles in solution. *Phys. Chem. Chem. Phys.* **2011**, *13*, 8881–8888.

(33) Turnbull, K. M.; Rahman, S. Endosperm texture in wheat. *J. Cereal Sci.* **2002**, *36*, 327–337.